

## RESEARCH ARTICLE

10.1002/2016JA023451

## Key Points:

- Test particle simulations of nonlinear resonances between radiation belt ultrarelativistic electrons and oblique EMIC waves
- Higher wave obliquity allows stronger (weaker) nonlinearity of harmonic (fundamental) cyclotron resonances
- Increase of wave obliquity tends to reduce the differences between test particle and quasi-linear total transport coefficients

## Correspondence to:

Z. Su,  
szpe@mail.ustc.edu.cn

## Citation:

Wang, G., Z. Su, H. Zheng, Y. Wang, M. Zhang, and S. Wang (2017), Nonlinear fundamental and harmonic cyclotron resonant scattering of radiation belt ultrarelativistic electrons by oblique monochromatic EMIC waves, *J. Geophys. Res. Space Physics*, 122, 1928–1945, doi:10.1002/2016JA023451.

Received 12 SEP 2016

Accepted 1 FEB 2017

Accepted article online 4 FEB 2017

Published online 21 FEB 2017

## Nonlinear fundamental and harmonic cyclotron resonant scattering of radiation belt ultrarelativistic electrons by oblique monochromatic EMIC waves

Geng Wang<sup>1,2,3</sup>, Zhenpeng Su<sup>1,2</sup> , Huinan Zheng<sup>1,2</sup> , Yuming Wang<sup>1,2</sup> , Min Zhang<sup>1,4</sup>, and Shui Wang<sup>1,2</sup>

<sup>1</sup>CAS Key Laboratory of Geospace Environment, Department of Geophysics and Planetary Sciences, University of Science and Technology of China, Hefei, China, <sup>2</sup>Collaborative Innovation Center of Astronautical Science and Technology, University of Science and Technology of China, Hefei, China, <sup>3</sup>Mengcheng National Geophysical Observatory, School of Earth and Space Sciences, University of Science and Technology of China, Hefei, China, <sup>4</sup>Department of Mathematics and Physics, Anhui Jianzhu University, Hefei, China

**Abstract** Cyclotron resonant scattering by electromagnetic ion cyclotron (EMIC) waves has been considered to be responsible for the rapid loss of radiation belt high-energy electrons. For parallel-propagating EMIC waves, the nonlinear character of cyclotron resonance has been revealed in recent studies. Here we present the first study on the nonlinear fundamental and harmonic cyclotron resonant scattering of radiation belt ultrarelativistic electrons by oblique EMIC waves on the basis of test particle simulations. Higher wave obliquity produces stronger nonlinearity of harmonic resonances but weaker nonlinearity of fundamental resonance. Compared to the quasi-linear prediction, these nonlinear resonances yield a more rapid loss of electrons over a wider pitch angle range. In the quasi-linear regime, the ultrarelativistic electrons are lost in the equatorial pitch angle range  $\alpha_{eq} < 75^\circ$ , nearly independent of wave normal angle  $\psi$ . In contrast, the upper pitch angle cutoff of nonlinear losses tends to increase with the wave normal angle increasing, which is about  $\alpha_{eq} = 82^\circ$  at  $\psi = 0^\circ$  and  $\alpha_{eq} > 87.5^\circ$  at  $\psi = 20^\circ$  and  $40^\circ$ . At the resonant pitch angles  $\alpha_{eq} < 75^\circ$ , the difference between quasi-linear and nonlinear loss timescales tends to decrease with the wave normal angle increasing. At  $\psi = 0^\circ$  and  $20^\circ$ , the nonlinear electron loss timescale is 10% shorter than the quasi-linear prediction; at  $\psi = 40^\circ$ , the difference in loss timescales is reduced to <5%.

### 1. Introduction

Earth's outer radiation belt electrons exhibit complex dynamics during both storm [e.g., Reeves *et al.*, 1998; Friedel *et al.*, 2002; Millan and Thorne, 2007; Anderson *et al.*, 2015] and nonstorm [Su *et al.*, 2014a, 2015, 2016] times. To resolve the precise loss mechanisms for these high-energy electrons is an important challenge of radiation belt research. In the early works [Dessler and Karplus, 1961; McIlwain, 1966], outward adiabatic transport was proposed to explain the electron flux dropout during geomagnetic storms (with the buildup of magnetospheric ring current) [Kim and Chan, 1997; Su *et al.*, 2010a]. Recently, some nonadiabatic loss processes have been identified, such as magnetopause shadowing [Li *et al.*, 1997; Desorgher *et al.*, 2000] and various wave-particle resonant [Horne and Thorne, 1998; Summers *et al.*, 1998; Green *et al.*, 2004; Thorne, 2010; Elkington *et al.*, 1999; Shprits *et al.*, 2006; Loto'Aniu *et al.*, 2010; Su *et al.*, 2015; Breneman *et al.*, 2015; Zhu *et al.*, 2015; Gao *et al.*, 2016] and nonresonant [Qin and Shalchi, 2009; Ragot, 2012; Lemons, 2012; Camporeale, 2015; Chen *et al.*, 2016] interactions. These nonadiabatic mechanisms can act not only in storm times [e.g., Bortnik *et al.*, 2006; Su *et al.*, 2011a; Turner *et al.*, 2012, 2014; Hudson *et al.*, 2014] but also in nonstorm times [Su *et al.*, 2016].

Electromagnetic ion cyclotron (EMIC) waves have long been considered to yield the rapid precipitation loss of radiation belt relativistic and ultrarelativistic electrons through cyclotron resonant pitch angle scattering [e.g., Summers and Thorne, 2003; Bortnik *et al.*, 2006; Summers *et al.*, 2007; Miyoshi *et al.*, 2008; Ukhorskiy *et al.*, 2010; Su *et al.*, 2011a, 2016; Kersten *et al.*, 2014; Usanova *et al.*, 2014; Engebretson *et al.*, 2015; Rodger *et al.*, 2015; He *et al.*, 2016; Zhang *et al.*, 2016]. This loss process is usually described by the quasi-linear theory [e.g., Albert, 2003; Summers and Thorne, 2003; Li *et al.*, 2007; Summers and Thorne, 2003; Li *et al.*, 2007; Jordanova *et al.*, 2008; Su *et al.*, 2016].

*Shprits et al.*, 2009a; *Su et al.*, 2010b, 2011b; *Mourenas et al.*, 2016]. In fact, the EMIC waves typically have large amplitudes of 1–10 nT [Bräsy et al., 1998; Erlandson and Ukhorskiy, 2001; Meredith et al., 2003; Fraser et al., 2010, Pickett et al., 2010; Omura et al., 2010], essentially violating the assumption of small wave amplitudes in the quasi-linear theory [Kennel and Engelmann, 1966; Lyons et al., 1971; Lyons, 1974; Horne and Thorne, 1998; Summers et al., 1998].

For parallel-propagating EMIC waves, several test particle studies on the nonlinear cyclotron resonance have been performed [e.g., Albert and Bortnik, 2009; Su et al., 2012, 2013a; Omura and Zhao, 2012; Zhu et al., 2012]. *Albert and Bortnik* [2009] showed that large amplitude EMIC waves can cause the nonlinear phase bunching and trapping of radiation belt electrons. The corresponding transport coefficients were found to significantly deviate from the quasi-linear prediction in both uniform [Liu et al., 2010, 2012] and dipolar [Su et al., 2012, 2013b] magnetic fields. *Omura and Zhao* [2012] emphasized the importance of phase trapping driven by EMIC rising-tone emissions for the loss of relativistic electrons over a wide pitch angle range.

Previous statistical studies have shown that the oblique EMIC waves with wave normal angles up to  $\psi = 80^\circ$  can frequently occur in both the outer ( $L > 6$ ) [Min et al., 2012] and inner ( $2 < L < 6$ ) [Saikin et al., 2015] magnetosphere. Recently, *Wang et al.* [2016] analyzed the nonlinear Landau resonant scattering of near-equatorially trapped radiation belt electrons driven by oblique EMIC waves. However, the potential nonlinear cyclotron resonance driven by oblique EMIC waves remains to be examined. In this study, we address the following two questions: (1) Can the fundamental and harmonic cyclotron resonance exhibit a significant nonlinearity for oblique EMIC waves? (2) How large is the difference between test particle and quasi-linear electron loss characteristics for oblique EMIC waves?

## 2. Numerical Model

### 2.1. Test Particle Model

We use the test particle code of *Su et al.* [2014b] to investigate the resonant interaction between monochromatic EMIC waves and ultrarelativistic electrons in the radiation belt. The basic equations are written as

$$\frac{d\mathbf{r}}{dt} = \frac{\mathbf{p}}{\gamma m}, \quad (1)$$

$$\frac{d\mathbf{p}}{dt} = q \left[ \mathbf{E}_w + \frac{\mathbf{p}}{\gamma m} \times (\mathbf{B}_0 + \mathbf{B}_w) \right]. \quad (2)$$

Following early works [e.g., *Inan et al.*, 1978; *Bell*, 1984], we ignore the curvature of background magnetic field and construct a “magnetic bottle” configuration

$$\mathbf{B}_0 = -\frac{x}{2} \frac{dB_D}{dz} \mathbf{e}_x - \frac{y}{2} \frac{dB_D}{dz} \mathbf{e}_y + B_D \mathbf{e}_z, \quad (3)$$

where  $z$  is the dipole field line length (depending on magnetic shell  $L$  and magnetic latitude  $\lambda$ ) and  $B_D$  is dipole field strength. For ultrarelativistic electrons, the bounce period ( $\sim 0.5$  s) is much shorter than the drift period ( $\sim 5$  mins), and the gyroradius (tens of kilometers) is small compared to the Earth’s radius (6376 km). This magnetic bottle approximation should not lead to significant errors in the simulations. Test electrons are characterized by charge  $q$ , rest mass  $m$ , position vector  $\mathbf{r}$ , local pitch angle  $\alpha$ , gyro phase

$$\varphi = -\int \frac{\Omega}{\gamma} dt = -\int \frac{qB_D}{\gamma m} dt, \quad (4)$$

and relativistic momentum vector

$$\mathbf{p} = p(\sin \alpha \cos \varphi \mathbf{e}_x + \sin \alpha \sin \varphi \mathbf{e}_y + \cos \alpha \mathbf{e}_z). \quad (5)$$

A monochromatic EMIC wave is characterized by angular frequency  $\omega$ , normal angle  $\psi$ , wave vector

$$\mathbf{k} = k \sin \psi \mathbf{e}_x + k \cos \psi \mathbf{e}_z, \quad (6)$$

wave phase

$$\phi = \int \mathbf{k} \cdot d\mathbf{r} - \int \omega dt, \quad (7)$$

electromagnetic fields

$$\mathbf{E}_w = -E_w^x \sin \phi \mathbf{e}_x - E_w^y \cos \phi \mathbf{e}_y - E_w^z \sin \phi \mathbf{e}_z, \quad (8)$$

$$\mathbf{B}_w = B_w^x \cos \phi \mathbf{e}_x - B_w^y \sin \phi \mathbf{e}_y + B_w^z \cos \phi \mathbf{e}_z, \quad (9)$$

and time-averaged Poynting flux

$$\overline{\mathbf{S}_w} = \frac{1}{2\mu_0} [ - (E_w^y B_w^z + E_w^z B_w^y) \mathbf{e}_x + (E_w^x B_w^y + E_w^y B_w^x) \mathbf{e}_z ]. \quad (10)$$

To qualitatively describe the nonlinear resonance process, we introduce two variables  $v$  and  $\eta$  [e.g., *Inan et al.*, 1978; *Bell*, 1984; *Bortnik et al.*, 2008; *Omura et al.*, 2008; *Tao and Bortnik*, 2010; *Su et al.*, 2014b]

$$v = \frac{d\eta}{dt} = \frac{l\Omega}{\gamma} + \frac{kp}{\gamma m} \cos \psi \cos \alpha - \omega. \quad (11)$$

The variable  $v$  equals zero at the  $l$  order resonance point

$$\omega - \frac{kp}{\gamma m} \cos \psi \cos \alpha = \frac{l\Omega}{\gamma}. \quad (12)$$

The variable  $\eta$  is approximated as

$$\eta \approx \phi - l\varphi - kx \sin \psi, \quad (13)$$

which can be interpreted as the difference between wave phase  $\phi$  and harmonic gyrophase  $l\varphi$  at the guiding center ( $x = 0$ ). Differentiating both sides of the equation (11) with respect to time  $t$  yields

$$\frac{d^2\eta}{dt^2} = \frac{dv}{dt} = \omega_t^2 [\text{Sign}(\vartheta) \sin \eta + S], \quad (14)$$

with the detailed expressions of  $S$ ,  $\omega_t$ , and  $\vartheta$  listed in our previous work [*Su et al.*, 2014b]. The absolute value of  $S$  at the resonance point is named as the “inhomogeneity parameter”  $S_r$  [*Omura et al.*, 2008]. As discussed in previous theoretical works [e.g., *Matsumoto and Omura*, 1981; *Summers and Omura*, 2007; *Omura et al.*, 2008; *Albert and Bortnik*, 2009; *Su et al.*, 2012, 2013b; *Zhu et al.*, 2012], wave-particle interaction can exhibit obvious nonlinearity when  $S_r \sim 1$  but become linear when  $S_r > 1$ .

In the test particle simulations, the bounce-averaged advection  $\langle A_{\alpha_{eq}}^{\text{TP}} \rangle$  and diffusion  $\langle D_{\alpha_{eq}\alpha_{eq}}^{\text{TP}} \rangle$  coefficients in equatorial pitch angle  $\alpha_{eq}$  can be evaluated as [*Schulz and Lanzerotti*, 1974; *Lyons and Williams*, 1984; *Liu et al.*, 2010, 2012; *Su et al.*, 2012, 2013b]

$$\langle A_{\alpha_{eq}}^{\text{TP}} \rangle = \overline{\frac{\Delta \alpha_{eq}}{\Delta t}}, \quad (15)$$

$$\langle D_{\alpha_{eq}\alpha_{eq}}^{\text{TP}} \rangle = \overline{\frac{(\Delta \alpha_{eq} - \overline{\Delta \alpha_{eq}})^2}{2\Delta t}}, \quad (16)$$

where  $\Delta t$  is the bounce period of test electrons,  $\Delta \alpha_{eq}$  is the net change in equatorial pitch angle during one bounce period, and the overline represents the averaging over initial gyrophase  $\varphi_0$  and latitude  $\lambda_0$ .

## 2.2. Quasi-Linear Theory

In the quasi-linear theory, the pitch angle diffusion equation can be written as [*Schulz and Lanzerotti*, 1974; *Lyons and Williams*, 1984]

$$\frac{\partial F}{\partial t} = \frac{1}{G} \frac{\partial}{\partial \alpha_{eq}} \left[ G \left( \langle D_{\alpha_{eq}\alpha_{eq}}^{\text{QL}} \rangle \frac{\partial F}{\partial \alpha_{eq}} \right) \right], \quad (17)$$

$$G = p^2 T(\alpha_{eq}) \sin \alpha_{eq} \cos \alpha_{eq}, \quad (18)$$

$$T \approx 1.30 - 0.56 \sin \alpha_{eq}, \quad (19)$$

with the electron phase space density  $F$  and the bounce-averaged diffusion coefficient in equatorial pitch angle  $\langle D_{\alpha_{eq}\alpha_{eq}}^{\text{QL}} \rangle$  depending on the wave properties and background plasma. Equation (17) can be rewritten into the advection-diffusion form [*Schulz and Lanzerotti*, 1974; *Liu et al.*, 2012]

$$\frac{\partial F}{\partial t} = -\frac{1}{G} \frac{\partial}{\partial \alpha_{eq}} \left( G \langle A_{\alpha_{eq}}^{\text{QL}} \rangle F \right) + \frac{1}{G} \frac{\partial^2}{\partial \alpha_{eq}^2} \left( G \langle D_{\alpha_{eq}\alpha_{eq}}^{\text{QL}} \rangle F \right), \quad (20)$$

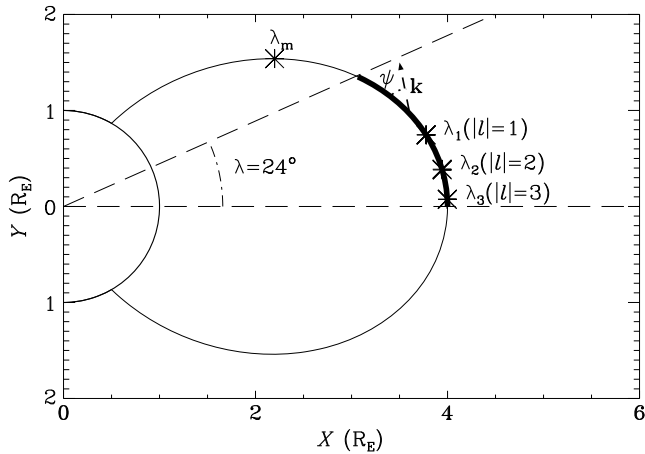


**Figure 1.** Schematic diagram of EMIC waves, linear resonance latitudes, and electron mirror point in the Northern Hemisphere.

with the inherent bounce-averaged advection coefficient in equatorial pitch angle  $\langle A_{\alpha_{eq}}^{QL} \rangle$

$$\langle A_{\alpha_{eq}}^{QL} \rangle = \frac{1}{G} \frac{\partial}{\partial \alpha_{eq}} (G \langle D_{\alpha_{eq} \alpha_{eq}}^{QL} \rangle). \quad (21)$$

For a monochromatic wave with the time-averaged amplitude  $\overline{B_w} = \sqrt{\frac{B_w^x + B_w^y + B_w^z}{2}}$ , the bounce-averaged diffusion coefficient for  $l$ -order cyclotron resonance is given as [Albert, 2010]

$$\begin{aligned} \langle D_{\alpha_{eq} \alpha_{eq}}^{QL} \rangle_l &= \frac{\pi \Omega^2 |\cos \alpha| \cos^7 \lambda \overline{B_w}^2}{2 \gamma^2 T(\alpha_{eq}) \cos^2 \alpha_{eq} B_D^2} \Phi_l^2 \\ &\times \left( \cos \psi - \frac{\gamma m}{p} \frac{\omega}{k} \cos \alpha \right)^2 \left| \frac{\partial}{\partial \lambda} \left( \frac{k p \cos \psi \cos \alpha}{\gamma m} + \frac{l \Omega}{\gamma} \right) \right|^{-1}, \end{aligned} \quad (22)$$

$$\begin{aligned} \Phi_l^2 &= \left[ \left( \frac{2D}{n^2 - S} \right)^2 + \left( \frac{2P \cos \psi}{P - n^2 \sin^2 \psi} \right)^2 \right]^{-1} \\ &\times \left[ \left( \frac{n^2 - L}{n^2 - S} \right) J_{l+1}(\beta) + \left( \frac{n^2 - R}{n^2 - S} \right) J_{l-1}(\beta) + \frac{n^2 \cot \alpha \sin 2\psi}{P - n^2 \sin^2 \psi} J_l(\beta) \right]^2, \end{aligned} \quad (23)$$

where all the quantities without subscript "eq" are evaluated at the resonance location. The equatorial resonance curve (along which  $\left| \frac{\partial}{\partial \lambda} \left( \frac{k p \cos \psi \cos \alpha}{\gamma m} + \frac{l \Omega}{\gamma} \right) \right| = 0$ ) is a singular line of both the analytical advection and diffusion coefficients, and the line  $\alpha_{eq} = 0$  (where  $G = 0$ ) is the other singular line of the analytical advection coefficient.

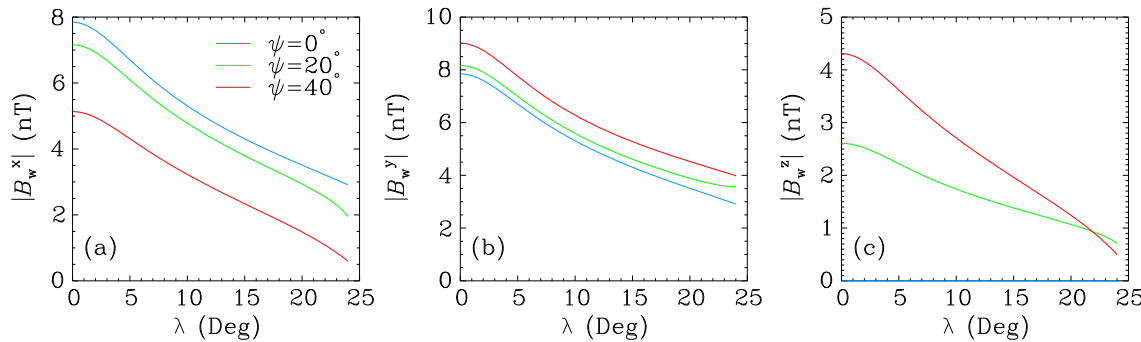


**Figure 2.** Latitudinal variation of wave component (a)  $|B_w^x|$ , (b)  $|B_w^y|$ , and (c)  $|B_w^z|$  with different wave normal angles  $\psi=0^\circ$  (blue),  $20^\circ$  (green) and  $40^\circ$  (red).

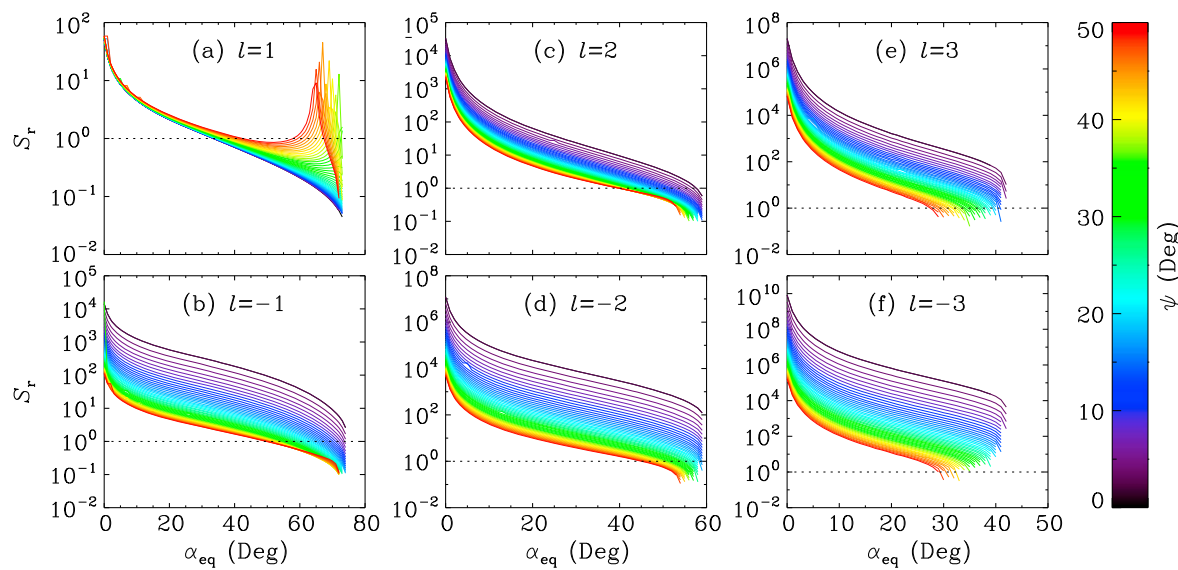


**Figure 3.** Dependence of inhomogeneity parameter  $S_r$  on equatorial pitch angle  $\alpha_{\text{eq}}$  with wave normal angles  $\psi = 0^\circ - 50^\circ$  (color coded) at resonance orders  $l = \pm 1, \pm 2$ , and  $\pm 3$ .

### 3. Results

Wave-particle interactions are investigated in the core of outer electron radiation belt ( $L = 4$ ). The equatorial ratio between plasma frequency and electron gyrofrequency is set to be 15 (typical value in the high-density plasmasphere) [Albert and Bortnik, 2009]. Background ion compositions are taken to be 77%  $\text{H}^+$  + 20%  $\text{He}^+$  + 3%  $\text{O}^+$  (typical values during storm times) [Jordanova et al., 2008]. Monochromatic EMIC waves with frequency  $\omega$  are assumed to generate at the equator and propagate toward higher latitudes ( $|\lambda| \leq 24^\circ$  to confine the wave in helium band) with the constant Poynting flux  $\bar{S}_w$ . The wave frequency is set to be close to the Helium ion gyrofrequency  $\omega = 0.96\Omega_{\text{He}}$  with a relatively large wave number  $k$  [Summers, 2005; Albert and Bortnik, 2009; Su et al., 2012], allowing the occurrence of both fundamental and harmonic resonances (see equation (24)). Previous statistical study [Loto'Aniu et al., 2005] found that Poynting fluxes of EMIC could reach up to  $25 \mu\text{W m}^{-2}$ . In subsections 3.1–3.3 and 3.5 the value of Poynting flux is specified as  $\bar{S}_w = 5 \mu\text{W m}^{-2}$  to investigate the nonlinear resonance process. Dependence of nonlinearity of wave-particle interaction on Poynting flux strength is shown in subsection 3.4. The kinetic energies of test electrons are taken to be 5 MeV throughout this study. As the electron energy decreases, the magnetic mirror force decreases and the nonlinearity of resonances at  $|l|=1$  increases [e.g., Albert and Bortnik, 2009; Su et al., 2012]. However, the decrease of electron energy reduces the parallel velocity, not conducive to the occurrence of  $|l| > 1$  resonances (see equation (24)).

#### 3.1. Normal Angle Dependence of Nonlinearity

Figure 1 presents the schematic distribution of waves, resonance latitudes  $\lambda_l$  ( $l = 1, 2, 3$ ), and mirror point  $\lambda_m$ . Since wave frequency  $\omega$  is much less than electron gyrofrequency  $\Omega$ , the cyclotron resonance condition can be approximated as

$$kp \cos \psi \cos \alpha = -lqB_D. \quad (24)$$

In the undisturbed orbit, electrons with the same equatorial pitch angles  $\alpha_{\text{eq}}$  and kinetic energies  $E_k$  should experience  $l$ th and  $-l$ th harmonic resonance almost at the same latitude  $\lambda_l$ . Higher  $|l|$  order harmonic resonances should occur at lower latitudes  $\lambda_l$  with larger parallel momentum  $p \cos \alpha$ .

Figure 2 shows the latitudinal variation of wave magnetic field components with fixed Poynting fluxes  $\bar{S}_w = 5 \mu\text{W m}^{-2}$ . Clearly, all these components decrease with latitude increasing. For parallel-propagating EMIC waves, the parallel component  $B_w^z$  is zero and the perpendicular components  $B_w^x$  and  $B_w^y$  decrease from 8 nT at  $\lambda = 0^\circ$  to 3 nT at  $\lambda = 24^\circ$ . Increase of wave obliquity leads to the decrease of  $B_w^x$  but the increase of  $B_w^y$  and  $B_w^z$ .

Figure 3 plots the inhomogeneity parameter  $S_r$  at different resonance orders  $l$ . With wave normal angle  $\psi$  increasing,  $S_r$  increases at  $l = 1$  but decreases at  $l \neq 1$ , suggesting that higher wave obliquity allows weaker

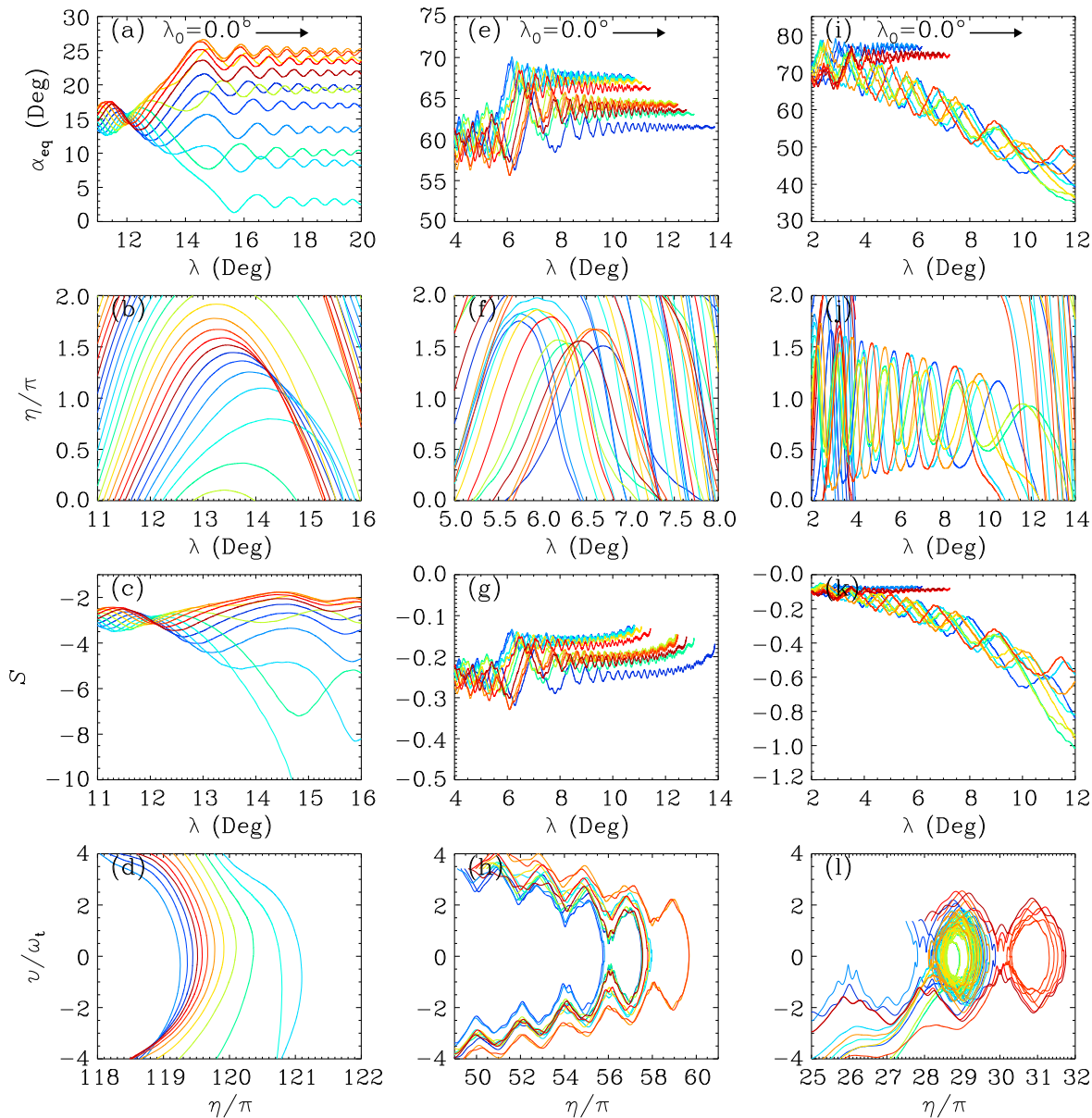


**Figure 4.** Electron trajectories (color coded according to the initial gyro phase  $\varphi_0$ ) of fundamental resonance ( $l = 1$ ) with wave normal angle  $\psi = 20^\circ$  in the (a, e, i)  $\lambda - \alpha_{\text{eq}}$ , (b, f, j)  $\lambda - \eta$ , (c, g, k)  $\lambda - S_r$ , and (d, h, l)  $\eta - v$  planes. Three columns correspond to three examples initialized at different equatorial pitch angles and latitudes. The black arrows represent the direction of electron motion.

nonlinearity of fundamental resonance but stronger nonlinearity of other harmonic resonances. As  $\alpha_{\text{eq}}$  increases,  $S_r$  for both fundamental and harmonic resonances decreases significantly. Note that  $S_r$  of fundamental resonance for EMIC waves with  $\psi > 30^\circ$  has a singularity around  $\alpha_{\text{eq}} = 70^\circ$  [Bell, 1984].  $S_r$  at positive resonance orders  $l$  appears to be much larger than that at corresponding negative resonance orders  $-l$  and higher absolute resonance orders  $|l|$  correspond to larger  $S_r$ . These results indicate that nonlinear resonance is favored by a large  $\alpha_{\text{eq}}$  and a small positive  $l$ . In the following subsections 3.2–3.4, we focus on the nonlinear resonances at  $|l| = 1$  and 2.

### 3.2. Fundamental Cyclotron Resonance

Figure 4 gives three examples of fundamental resonance  $l = 1$  with wave normal angle  $\psi = 20^\circ$ . In each example, 12 test electrons with the initial gyrophase  $\varphi_0$  uniformly distributed in the range of  $0-2\pi$  at the latitude  $\lambda_0$  are launched toward the Northern Hemisphere. The resonance occurs around the stationary point  $(d\eta/d\lambda = 0)$  of  $\eta - \lambda$  curve. The resonance phase  $\eta_r$  largely determines the sign of equatorial pitch angle

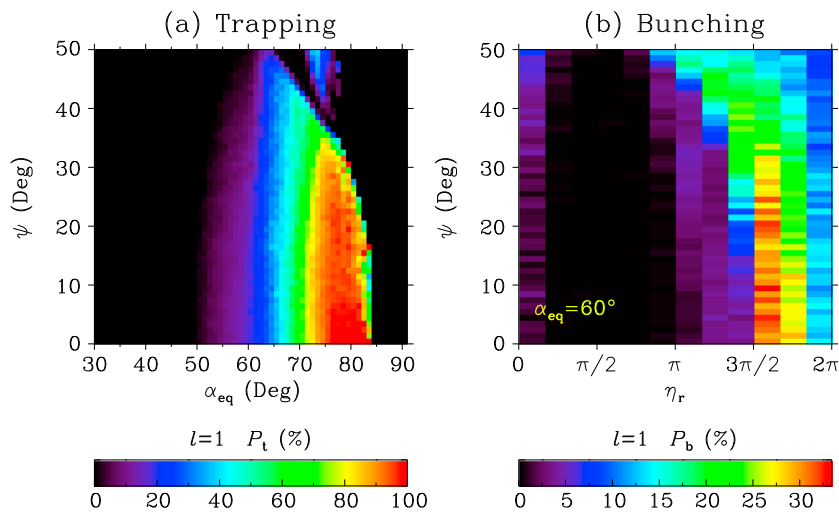


**Figure 5.** Probability distribution of (a) phase trapping in  $\alpha_{\text{eq}} - \psi$  plane and (b) phase bunching with  $\alpha_{\text{eq}} = 60^\circ$  in  $\eta_r - \psi$  plane for fundamental cyclotron resonance.

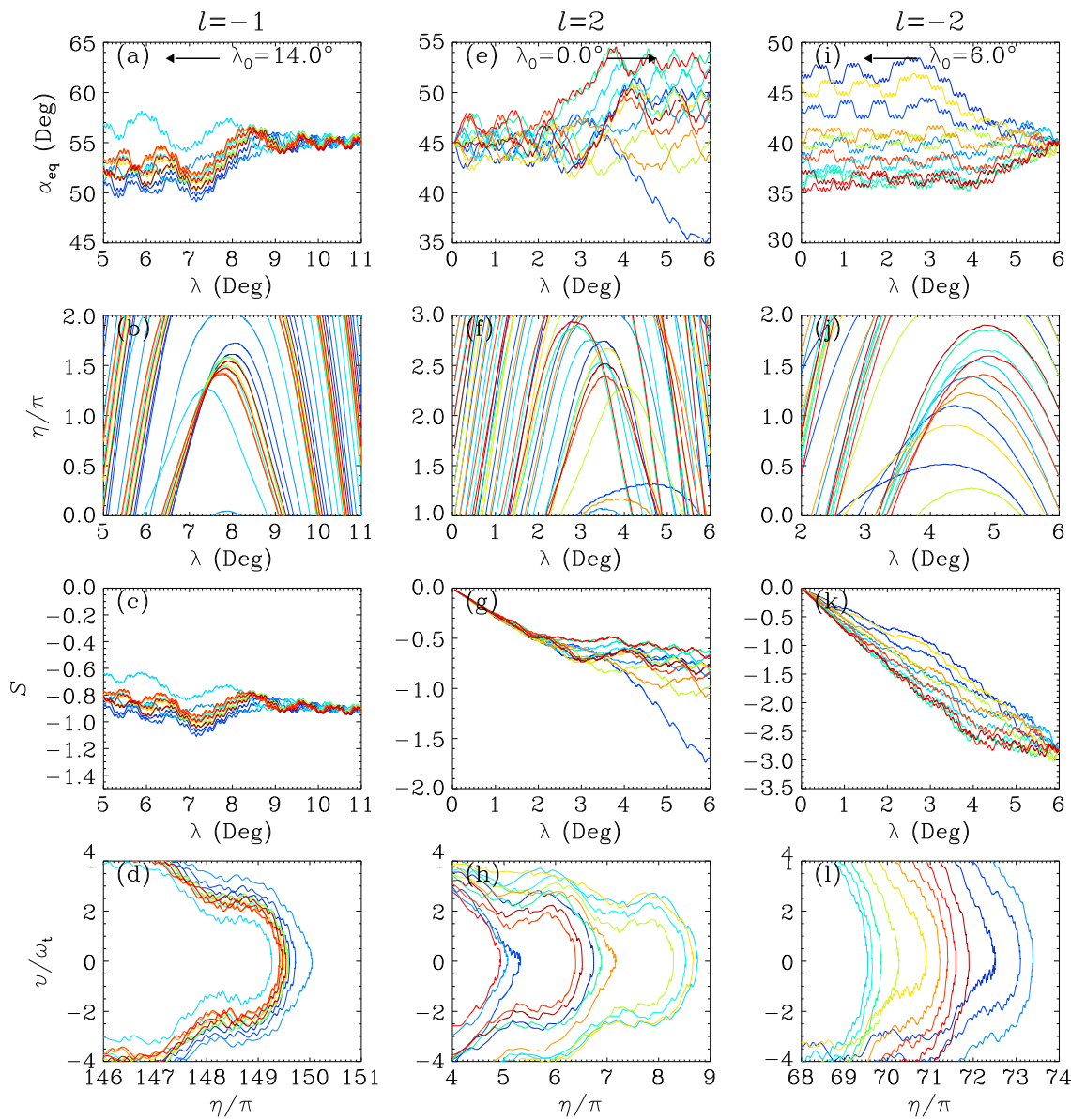
change  $\Delta\alpha_{\text{eq}}$ . The first example represents the quasi-linear resonant scattering, during which both resonance phases  $\eta_r$  and equatorial pitch angle changes  $\Delta\alpha_{\text{eq}}$  of test electrons appear to be nearly random. In the second example, the resonant phases are bunched in the range of  $\pi - 2\pi$ . As a result, the phase bunching during  $l = 1$  resonance mainly results in the positive changes of equatorial pitch angle  $\Delta\alpha_{\text{eq}}$ , not conducive to the loss of electrons. For the third example, a part of electron trajectories in the  $\eta_r - \psi$  plane turn to be closed, which is known as the phase trapping. These phase-trapped electrons experience a series of resonances, and their equatorial pitch angles are reduced from  $\alpha_{\text{eq}} = 70^\circ$  down to  $40^\circ$  within 1/4 bounce period. This phase trapping can effectively transport electrons toward loss cone, favoring the loss of electrons.

Figure 5a shows the occurrence rate of phase trapping as a function of equatorial pitch angle  $\alpha_{\text{eq}}$  and normal angle  $\psi$ . At an arbitrary grid point  $(\alpha_{\text{eq}}, \psi)$ ,  $N = 24 \times 40$  test electrons are randomly distributed in the region of  $\varphi_0 \in [0, 2\pi] \times \lambda_0 \in [0, \lambda_m]$  and launched toward the northern mirror point. The trapping occurrence rate is directly defined as  $P_t = N_t/N_1$  with the number  $N_t$  of electrons experiencing only  $l = 1$  resonance and the number  $N_b$  of electrons experiencing only  $l = 1$  phase trapping. The peak trapping rate occurs around  $\alpha_{\text{eq}} = 77^\circ$  with  $\psi = 0^\circ$ . Clearly, as wave normal angle  $\psi$  increases, the equatorial pitch angle interval with phase trapping shrinks and the phase trapping rate for a given  $\alpha_{\text{eq}}$  decreases. Figure 5b plots the probability distribution of resonance phases  $\eta_r$  of untrapped electrons with  $\alpha_{\text{eq}} = 60^\circ$  experiencing only  $l = 1$  resonance in the  $\eta_r - \psi$  space. The occurrence rate at a given grid point  $(\eta_r, \psi)$  is calculated as  $P_b = N_b/N_1$  with  $N_b$  representing the number of electrons in the bin  $\Delta\eta_r = \pi/6 \times \Delta\psi = 1^\circ$ . The increase of wave normal angle leads to the expansion of resonance phase interval (i.e., weakening of phase bunching effect). These results suggest that the nonlinear fundamental cyclotron resonance is generally favored for EMIC waves with small normal angles, consistent with the prediction of inhomogeneity parameter  $S_r$  (Figure 3).

### 3.3. Harmonic Cyclotron Resonances

Three examples of phase bunching for  $l = -1, 2$ , and  $-2$  harmonic cyclotron resonances with wave normal angles  $\psi = 45^\circ$  are shown in Figure 6. In each example, the resonance phases of test electrons tend to concentrate in the range  $\pi < \eta_r < 2\pi$ . The sign of equatorial pitch angle change  $\Delta\alpha_{\text{eq}}$  of phase bunched electrons depends on the resonance orders. Phase bunching favors the loss of electrons (producing negative  $\Delta\alpha_{\text{eq}}$ ) for  $l = -1$  and  $-2$ , but reduces the electron loss rate (producing positive  $\Delta\alpha_{\text{eq}}$ ) for  $l = 2$ . Figure 7 presents three examples of phase trapping for harmonic cyclotron resonances with normal angle  $\psi = 40^\circ$ . Contrary to phase bunching, phase trapping is not conducive to electron loss for  $l = -1$  and  $-2$  but promotes the electron loss for  $l = 2$ . Compared to fundamental resonance, harmonic resonances cause much weaker changes of equatorial pitch angles. For example, the maximum of  $|\Delta\alpha_{\text{eq}}|$  is about  $15^\circ$  for the  $l = 2$  phase trapping (Figure 7e) but increases to  $30^\circ$  for the  $l = 1$  phase trapping (Figure 4i).

The probability distributions of phase trapping and phase bunching during three harmonic resonances are provided in Figure 8. At an arbitrary grid point  $(\alpha_{\text{eq}}, \psi)$ ,  $N = 24 \times 40$  test electrons are initialized randomly in



**Figure 6.** Same as Figure 4 except for nonlinear phase bunching at harmonic cyclotron resonances with wave normal angle  $\psi = 45^\circ$ .

the region of  $\varphi_0 \in [0, 2\pi] \times \lambda_0 \in [0, \lambda_m]$ . They are launched toward the northern mirror point for the positive resonance orders but toward the equator for the negative resonance orders. For a specific resonance order  $l$ , we select the electrons undergoing the  $l$ -order resonance prior to other resonances, and then differentiate between  $l$ -order phase trapping and bunching, and finally obtain the corresponding occurrence rates. Clearly, the significant phase trapping and bunching can occur only for EMIC waves with large enough normal angles. The threshold values of normal angle for phase trapping are about  $\psi = 8^\circ, 5^\circ$ , and  $30^\circ$  at  $l = -1, 2$ , and  $-2$ , respectively. For phase bunching at  $\alpha_{eq} = 50^\circ$ , the threshold values of normal angle are about  $\psi = 30^\circ, 10^\circ$  and  $30^\circ$  at  $l = -1, 2$ , and  $-2$ , respectively.

### 3.4. Transport Coefficients

Figures 9 and 10 show the comparison between transport coefficients from quasi-linear theory and test particle simulation with wave Poynting flux  $\bar{S}_w = 0.01$  and  $5 \mu\text{W m}^{-2}$ . For the small amplitude waves (Figure 9), there is no obvious nonlinearity, and transport coefficients of two regimes agree well with each other

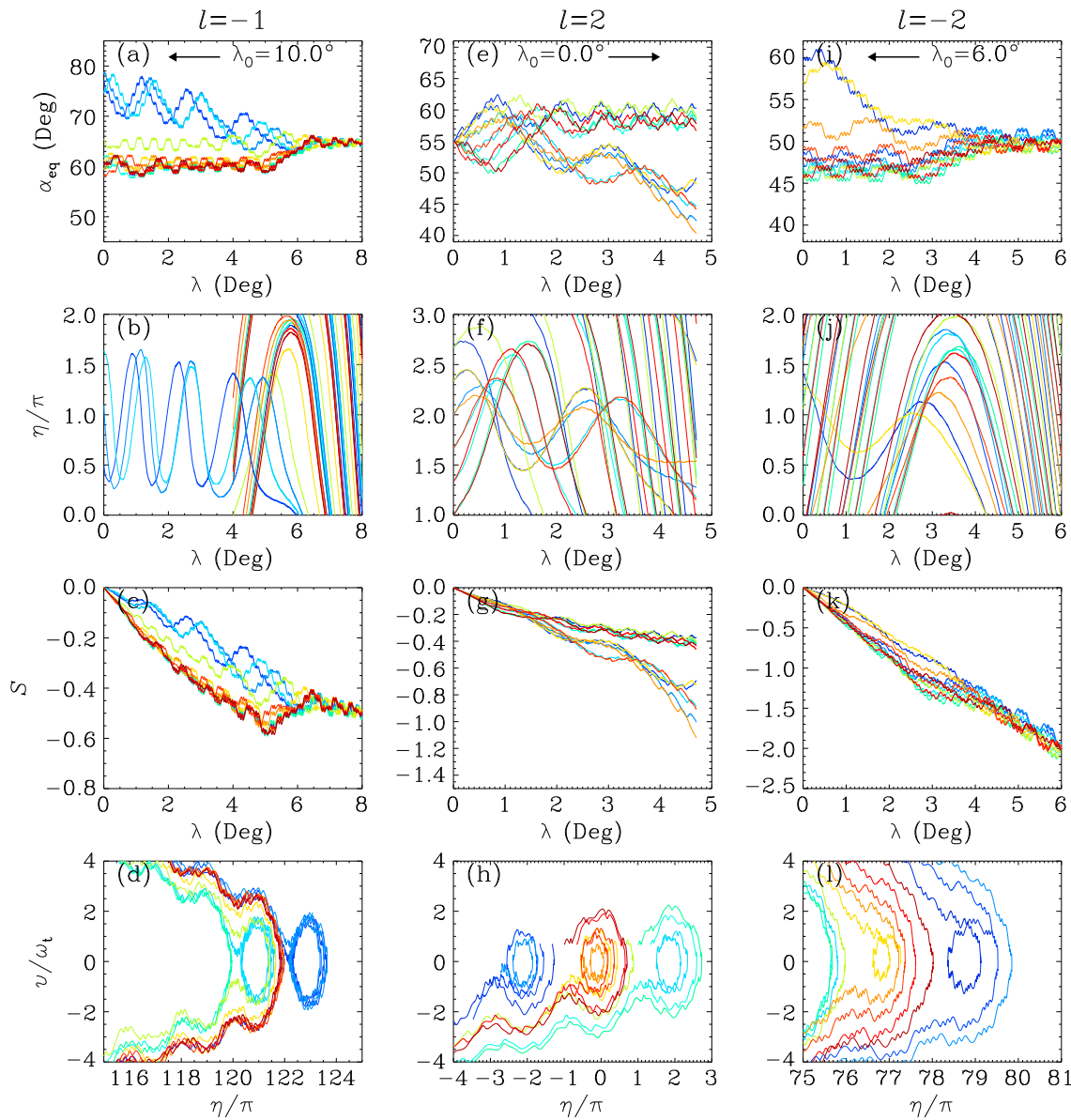


**Figure 7.** Same as Figure 4 except for nonlinear phase trapping at harmonic cyclotron resonances with wave normal angle  $\psi = 40^\circ$ .

(except around those singular points). For the large amplitude waves (Figure 10), strong nonlinearity arises and the test particle transport coefficients deviate significantly from the quasi-linear total transport coefficients particularly at the equatorial pitch angles  $\alpha_{\text{eq}} > 40^\circ$ .

Around  $\alpha_{\text{eq}} = 76^\circ$ , the test particle advection coefficients exhibit large negative values, contrary to the prediction of quasi-linear theory. Figure 11 presents a group of electron trajectories initialized at  $\lambda_0 = -5^\circ$  with wave normal angle  $\psi = 40^\circ$  during one bounce period. All the electrons experience the  $l = \pm 1$  cyclotron resonances while only about 1/3 electrons undergo the  $l = \pm 2$  cyclotron resonances. Phase trapping at  $l = 1$  and phase bunching at  $l = -1$  can be clearly identified. The net change of equatorial pitch angles is found to be predominantly produced by the  $l = 1$  phase trapping. As shown in Figure 5a, the decrease of normal angle increases the occurrence rate of phase trapping at  $l = 1$  and consequently increases the absolute values of advection coefficients (Figure 10).

In the equatorial pitch angle range  $\alpha_{\text{eq}} = 40^\circ - 60^\circ$ , the test particle advection coefficients become larger than the quasi-linear coefficients. Figure 12 exhibits the trajectories of electrons initialized with  $\alpha_{\text{eq}} = 58^\circ$ ,

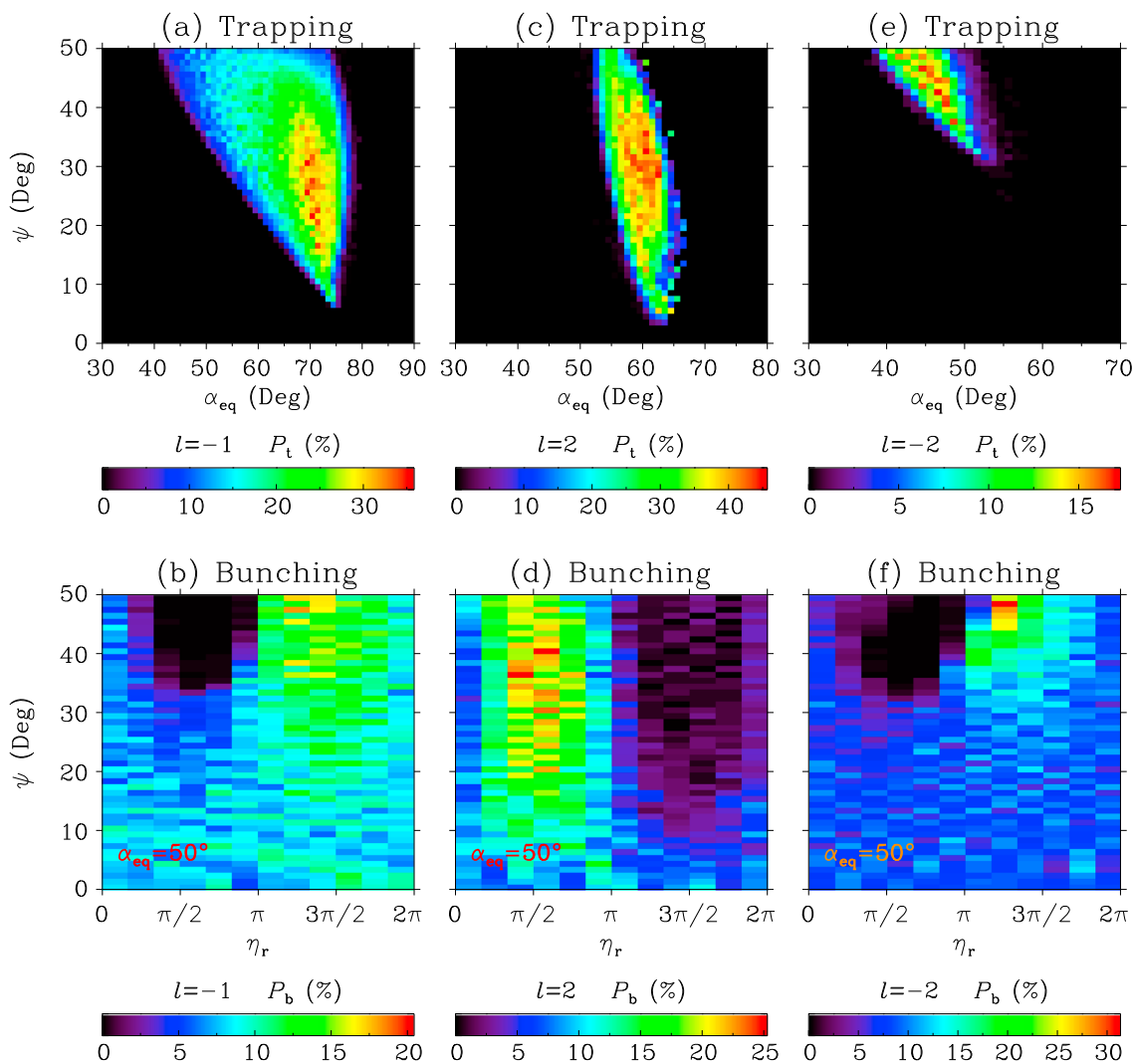


**Figure 8.** Same with Figure 5 except for harmonic cyclotron resonances.

$\psi = 40^\circ$  and  $\lambda_0 = -5^\circ$ . All these electrons experience the cyclotron resonances at  $l = \pm 1$  and  $\pm 2$ . Clearly, there exist phase trapping at  $l = -1$  and 2 and phase bunching at  $l = \pm 1$  and  $\pm 2$ . Absolute values of equatorial pitch angle changes  $|\Delta\alpha_{eq}|$  at different resonance orders are comparable, but the transport directions are dependent on the resonance orders (Figures 4, 6, and 7). Overlap of these nonlinear resonances leads to approximately random changes of equatorial pitch angles. The corresponding test particle transport coefficients become relatively close to the quasi-linear prediction. With normal angle decreasing, the nonlinearity decreases at the harmonic resonances (Figure 8) but increases at the fundamental resonance (Figure 5). The strong nonlinear phase bunching at  $l = 1$  can produce the positive advection coefficients at  $\alpha_{eq} = 40^\circ - 60^\circ$  (Figures 10a and 10c).

Figure 13 plots the dependence of test particle and quasi-linear diffusion coefficients (averaged over  $\alpha_{eq} = 20^\circ$  to  $50^\circ$ ) on the wave Poynting flux  $\bar{S}_w$ . In the quasi-linear regime, the diffusion coefficient is proportional to wave Poynting flux (see equation (22)). At each wave normal angle, there exists a threshold Poynting flux beyond which the test particle diffusion coefficient starts to deviate from the quasi-linear prediction. This threshold Poynting flux tends to increase as the wave normal angle increases. For  $\psi = 0^\circ$ ,  $20^\circ$ , and  $40^\circ$ , the corresponding threshold values are about 1, 3, and  $5 \mu\text{W m}^{-2}$ , respectively.

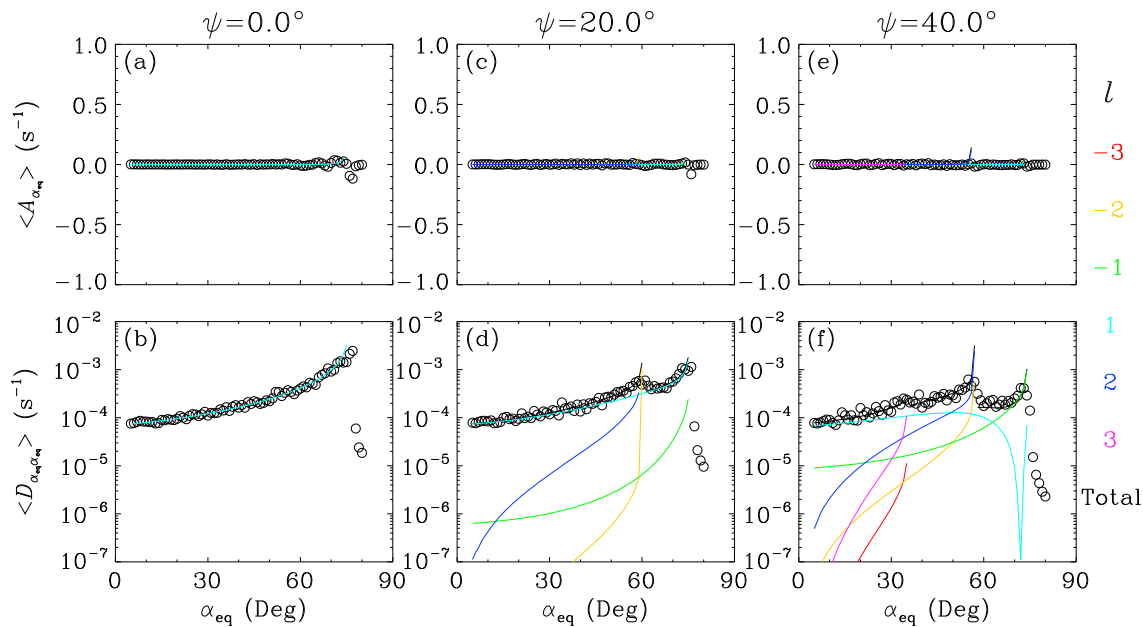


**Figure 9.** Bounce-averaged pitch angle (a, c, e) advection and (b, d, f) diffusion coefficients from test particle simulation (circles) and quasi-linear theory (lines) with wave Poynting flux  $\bar{S}_w = 0.01 \mu\text{W m}^{-2}$ . Line color helps differentiate among the quasi-linear transport coefficients at different resonance orders and the total coefficients.

### 3.5. Electron Phase Space Density Evolution

Figure 14 compares the temporal evolutions of quasi-linear and test particle electron phase space densities. The initial phase space density  $F$  is assumed to be uniform outside the loss cone. The bounce-averaged diffusion coefficients are directly input into the quasi-linear diffusion equation (17) with an additional term  $-F/\tau_L$  in the bounce loss cone ( $\tau_L$  is set to be a quarter of bounce period [Shprits et al., 2009b]). The corresponding boundary conditions are given as  $\partial F/\partial \alpha_{eq} = 0$  at  $\alpha_{eq} = 0^\circ$  and  $90^\circ$  [e.g., Shprits et al., 2009b; Su et al., 2009].

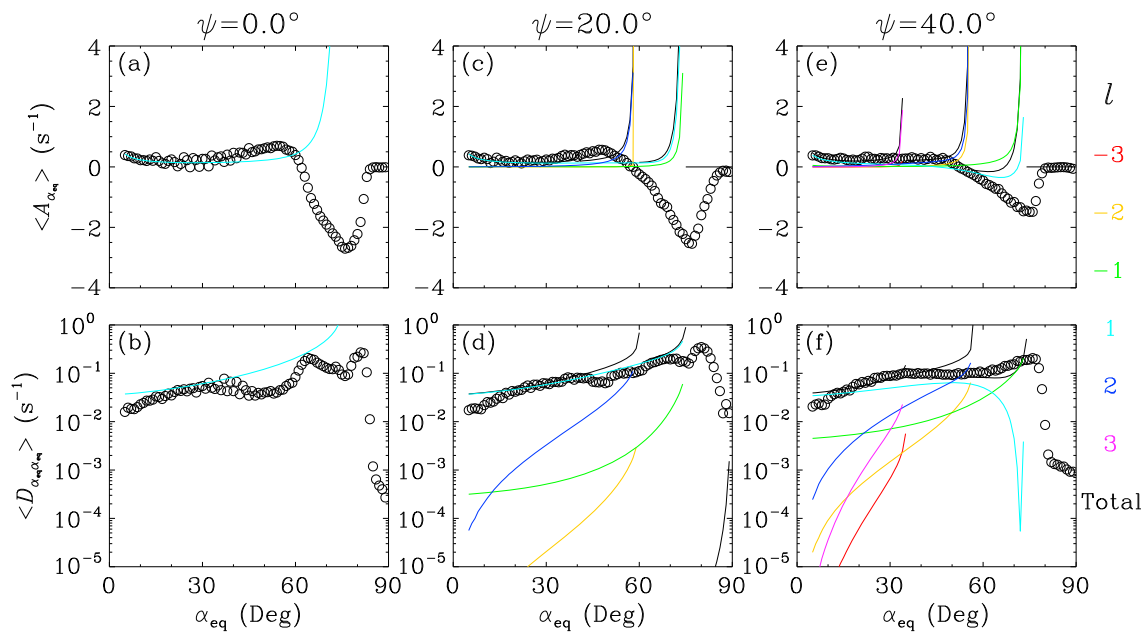


**Figure 10.** Same with Figure 9 except with wave Poynting flux  $\bar{S}_w = 5 \mu\text{W m}^{-2}$ .

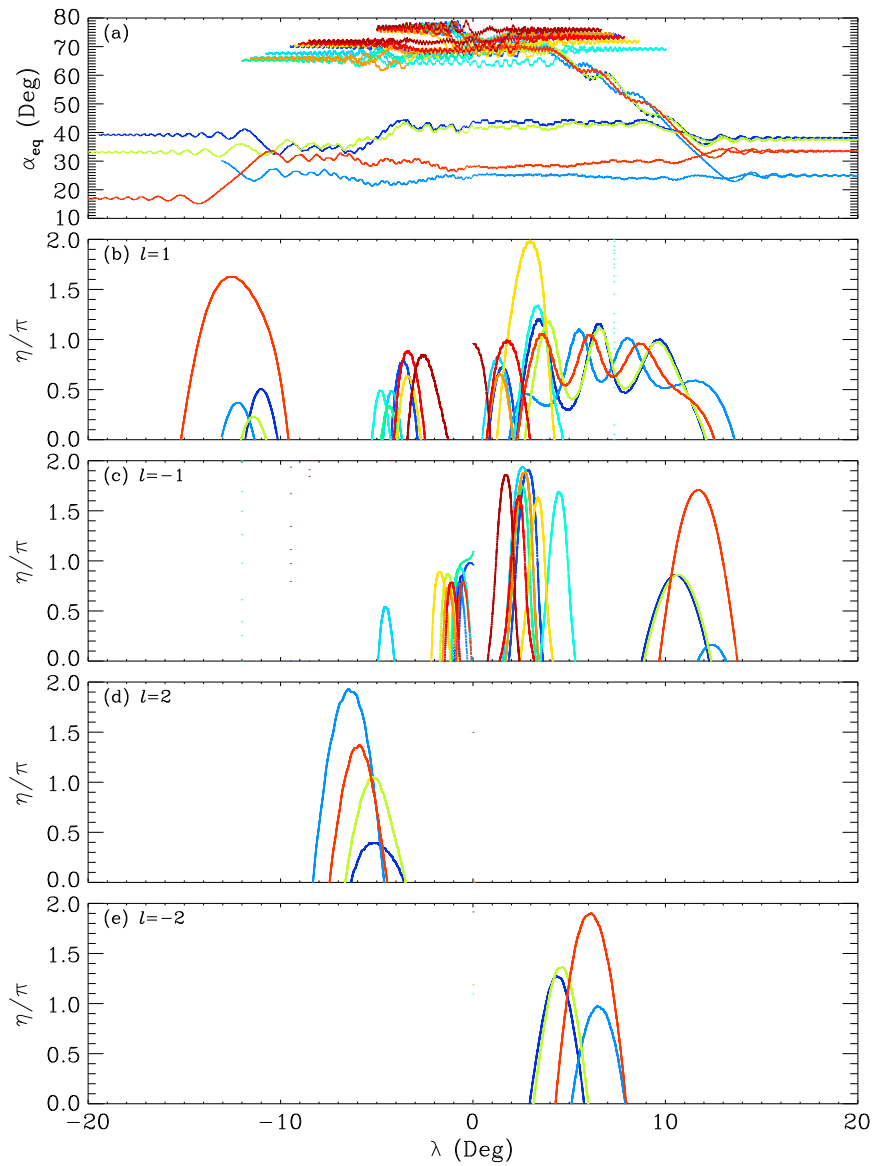


**Figure 11.** Trajectories of a group of test electrons (color-coded according to the initial gyro phase  $\varphi_0$ ) initialized with  $\alpha_{\text{eq}} = 76^\circ$  and  $\lambda_0 = -5^\circ$  for  $\psi = 40^\circ$  during a bounce period. In Figures 11b–11e, only the trajectories near resonance points are shown.

We launch  $24 \times 100 \times 85$  test electrons uniformly distributed in the space  $\varphi_0 \in [0, 2\pi] \times \lambda_0 \in [-\lambda_m, \lambda_m] \times \alpha_{\text{eq}} \in [5^\circ, 89^\circ]$  ( $\lambda_m$  is the mirror latitude). The initial phase space density of a test electron at  $\alpha_{\text{eq}} = \alpha_0$  is  $f_0 = \frac{1}{24 \times 100}$ , and at an arbitrary time, the phase space density of this test electron is determined as [Omura et al., 2015]

$$f(t, \alpha_{\text{eq}}) = \frac{G(p, \alpha_0)}{G(p, \alpha_{\text{eq}})} f_0. \quad (25)$$

with the weight function  $G$  given in equation (18). During the calculations, the test electrons with radial locations less than  $1 R_E$  are considered to be lost to the atmosphere. At the initial stage ( $t < 1$  s), the test particle phase space density profile exhibits a clear dip around  $\alpha_{\text{eq}} = 75^\circ$  due to the nonlinear phase trapping (Figure 10). As time goes on the test particle phase space density profiles are gradually flattened. The upper pitch angle cutoff of test electron losses is about  $82^\circ$  at  $\psi = 0^\circ$  and becomes  $>87.5^\circ$  at  $\psi = 20^\circ$  and  $40^\circ$ ,

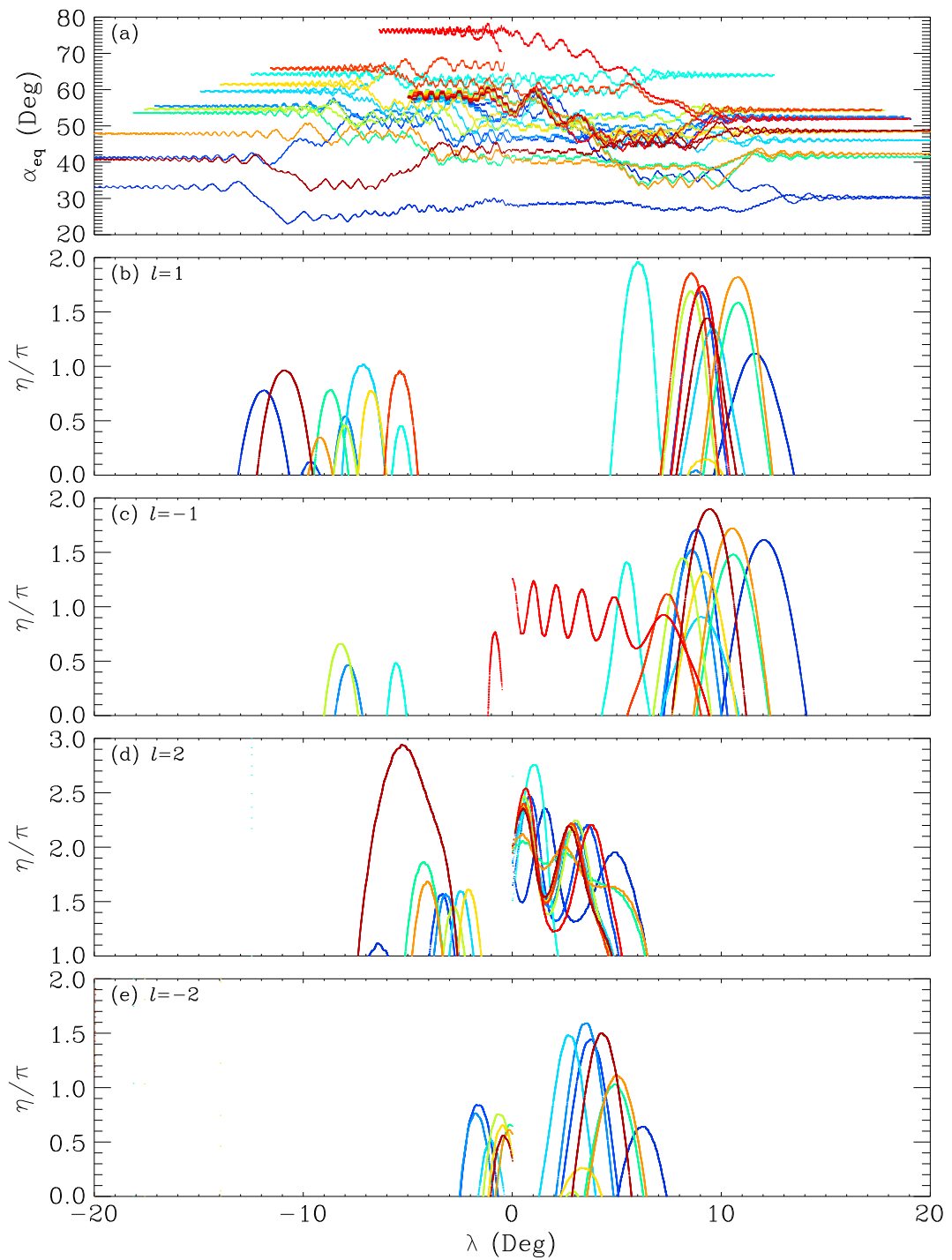


**Figure 12.** Same with Figure 11 except with the initial  $\alpha_{eq} = 58^\circ$ .

much larger than the quasi-linear prediction of  $\sim 75^\circ$  (nearly independent of wave normal angle  $\psi$ ). When  $\psi = 0^\circ$  and  $20^\circ$ , the electron phase space densities from the quasi-linear calculation at  $t = 30$  s and from the test particle simulation at  $t = 27$  s are roughly consistent with each other in the equatorial pitch angle range  $\alpha_{eq} < 75^\circ$ , indicating that the nonlinear electron loss timescale is 10% shorter than the quasi-linear prediction. When  $\psi = 40^\circ$ , the difference between the test particle and quasi-linear loss timescales is reduced to  $< 5\%$  in the equatorial pitch angle range  $\alpha_{eq} < 75^\circ$ .

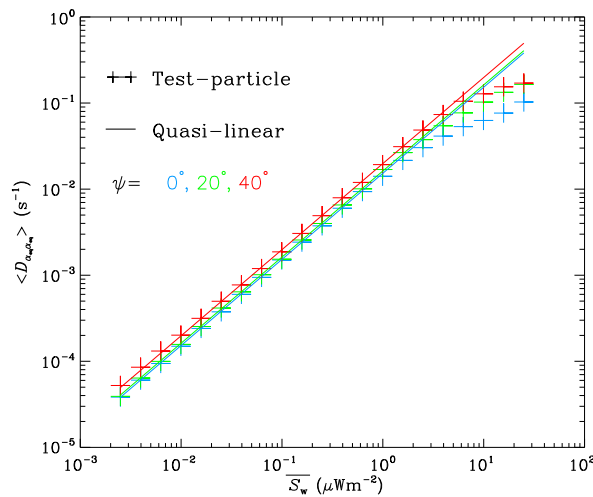


**Figure 13.** Dependence of quasi-linear (solid lines) and test particle (symbols) pitch angle diffusion coefficients on wave Poynting fluxes at different wave normal angles (color-coded).

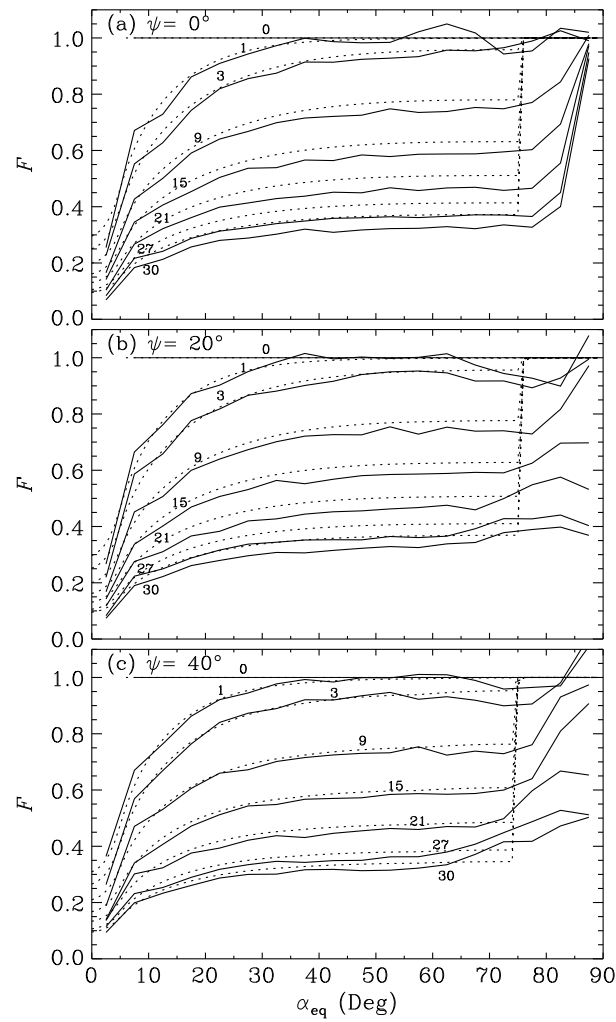


**Figure 14.** Temporal evolutions of electron phase space densities  $F$  (dependent on equatorial pitch angle  $\alpha_{\text{eq}}$ ) from the quasi-linear theory (dashed) and the test particle simulations (solid) at different wave normal angles (a)  $\psi = 0^\circ$ , (b)  $\psi = 20^\circ$  and (c)  $\psi = 40^\circ$ , respectively. The plotted profiles are at the time points 0 s, 1 s, 3 s, 9 s, 15 s, 21 s, 27 s, and 30 s, respectively.

## 4. Conclusions

Cyclotron resonant scattering by EMIC waves is widely believed to be an important physical mechanism responsible for the rapid loss of high-energy radiation belt electrons [Thorne and Kennel, 1971; Bortnik et al., 2006; Miyoshi et al., 2008; Su et al., 2011a, 2016]. Previous quasi-linear and test particle simulations [e.g., Li et al., 2007; Albert and Bortnik, 2009; Shprits et al., 2009a; Su et al., 2010c, 2012; Omura and Zhao, 2012] usually focused on the parallel-propagating EMIC waves. In fact, the oblique EMIC waves with wave normal angles up to  $\psi = 80^\circ$  can frequently occur in the inner ( $2 < L < 6$ ) magnetosphere [Saikin et al., 2015]. Here we present the first study of nonlinear cyclotron resonant scattering of ultrarelativistic ( $E_k = 5$  MeV) electrons by obliquely propagating monochromatic EMIC waves. Our principal conclusions are as follows:

1. Both fundamental ( $l = 1$ ) and harmonic ( $l = -1, 2$ , and  $-2$ ) cyclotron resonances can exhibit significant nonlinearity for oblique EMIC waves. Phase trapping at positive resonance orders ( $l = 1$  and  $2$ ) and phase bunching at negative resonance orders ( $l = -1$  and  $-2$ ) tend to transport electrons toward the loss cone, favoring the precipitation loss of electrons. In contrast, electrons experiencing phase trapping at negative resonance orders ( $l = -1$  and  $-2$ ) and phase bunching at positive resonance orders ( $l = 1$  and  $2$ ) are driven away from the loss cone. Test particle advection and diffusion coefficients are found to deviate significantly from the quasi-linear prediction especially at large pitch angles  $\alpha_{eq} > 40^\circ$ . As the wave normal angle increases, the differences between quasi-linear and test particle transport coefficients tend to be reduced. At  $\alpha_{eq} = 40^\circ - 60^\circ$ , the increase of wave normal angle leads to the overlapping of multiple nonlinear resonances with different transport directions and then randomizes the motion of resonant electrons, reducing the differences between transport coefficients of the two regimes. At  $\alpha_{eq} > 60^\circ$ , the nonlinear phase trapping at  $l = 1$  is dominant, which is unfavored for EMIC waves with large normal angles. Consequently, higher wave normal angles allow the weaker deviation of test particle transport coefficients from quasi-linear predictions at  $\alpha_{eq} > 60^\circ$ .
2. Compared to the quasi-linear prediction, these nonlinear resonances can produce a more rapid loss of ultrarelativistic electrons over a wider pitch angle range. Quasi-linear losses of ultrarelativistic electrons mainly occur in the equatorial pitch angle range  $\alpha_{eq} < 75^\circ$ , nearly independent of wave normal angle  $\psi$ . In the test particle simulations, the increase of wave normal angle tends to enlarge the upper pitch angle cut-offs of nonlinear losses. At  $\psi = 0^\circ$ , the upper pitch angle cutoff of nonlinear losses is about  $\alpha_{eq} = 82^\circ$ , and it increases to  $\alpha_{eq} > 87.5^\circ$  at  $\psi = 20^\circ$  and  $40^\circ$ . At the linear resonant pitch angles  $\alpha_{eq} < 75^\circ$ , increase of wave normal angle tends to reduce the difference between quasi-linear and nonlinear loss timescales. When  $\psi = 0^\circ$  and  $20^\circ$ , the nonlinear electron loss timescale is 10% shorter than the quasi-linear prediction; when  $\psi = 40^\circ$ , the difference in loss timescales is reduced to  $< 5\%$ .

## Acknowledgments

This work was supported by the National Natural Science Foundation of China grants 41422405, 41631071, 41274169, 41274174, 41631071, 41174125, 41131065, 41421063, 41231066, and 41304134; the Chinese Academy of Sciences grants KZCX2-EW-QN510 and KZZD-EW-01-4; the National Key Basic Research Special Foundation of China grant 2011CB811403; the Fundamental Research Funds for the Central Universities grant WK2080000077; and the foundation for Young Talents in College of Anhui Province grant 2013SQRL044ZD. The simulation data will be made available upon request to the corresponding author.

## References

- Albert, J. M. (2003), Evaluation of quasi-linear diffusion coefficients for EMIC waves in a multispecies plasma, *J. Geophys. Res.*, 108(A8), 1249, doi:10.1029/2002JA009792.
- Albert, J. M. (2010), Diffusion by one wave and by many waves, *J. Geophys. Res.*, 115, A00F05, doi:10.1029/2009JA014732.
- Albert, J. M., and J. Bortnik (2009), Nonlinear interaction of radiation belt electrons with electromagnetic ion cyclotron waves, *Geophys. Res. Lett.*, 36, L12110, doi:10.1029/2009GL038904.
- Anderson, B., R. Millan, G. D. Reeves, and R. H. W. Friedel (2015), Acceleration and loss of relativistic electrons during small geomagnetic storms, *Geophys. Res. Lett.*, 42, 10,113–10,119, doi:10.1002/2015GL066376.
- Bell, T. F. (1984), The nonlinear gyroresonance interaction between energetic electrons and coherent VLF waves propagating at an arbitrary angle with respect to the Earth's magnetic field, *J. Geophys. Res.*, 89, 905–918, doi:10.1029/JA089iA02p00905.
- Bortnik, J., R. M. Thorne, T. P. O'Brien, J. C. Green, R. J. Strangeway, Y. Y. Shprits, and D. N. Baker (2006), Observation of two distinct, rapid loss mechanisms during the 20 November 2003 radiation belt dropout event, *J. Geophys. Res.*, 111, A12216, doi:10.1029/2006JA011802.
- Bortnik, J., R. M. Thorne, and U. S. Inan (2008), Nonlinear interaction of energetic electrons with large amplitude chorus, *Geophys. Res. Lett.*, 35, L21102, doi:10.1029/2008GL035500.
- Bräysy, T., K. Mursula, and G. Marklund (1998), Ion cyclotron waves during a great magnetic storm observed by Freja double-probe electric field instrument, *J. Geophys. Res.*, 103, 4145–4156, doi:10.1029/97JA02820.
- Breneman, A., et al. (2015), Global-scale coherence modulation of radiation-belt electron loss from plasmaspheric hiss, *Nature*, 523, 193–195, doi:10.1038/nature14515.
- Camporeale, E. (2015), Resonant and nonresonant whistlers-particle interaction in the radiation belts, *Geophys. Res. Lett.*, 42, 3114–3121, doi:10.1002/2015GL063874.
- Chen, L., R. M. Thorne, J. Bortnik, and X.-J. Zhang (2016), Nonresonant interactions of electromagnetic ion cyclotron waves with relativistic electrons, *J. Geophys. Res. Space Physics*, 121, 9913–9925, doi:10.1002/2016JA022813.
- Desorgher, L., P. Bühl, A. Zehnder, and E. O. Flückiger (2000), Simulation of the outer radiation belt electron flux decrease during the March 26, 1995, magnetic storm, *J. Geophys. Res.*, 105, 21,211–21,224, doi:10.1029/2000JA900060.
- Dessler, A. J., and R. Karplus (1961), Some effects of diamagnetic ring currents on Van Allen radiation, *J. Geophys. Res.*, 66, 2289–2295, doi:10.1029/JZ066i008p02289.

- Elkington, S. R., M. K. Hudson, and A. A. Chan (1999), Acceleration of relativistic electrons via drift-resonant interaction with toroidal-mode Pc-5 ULF oscillations, *Geophys. Res. Lett.*, 26, 3273–3276, doi:10.1029/1999GL003659.
- Engebretson, M., et al. (2015), Van Allen probes, NOAA, GOES, and ground observations of an intense EMIC wave event extending over 12 h in magnetic local time, *J. Geophys. Res. Space Physics*, 120, 5465–5488, doi:10.1002/2015JA021227.
- Erlandson, R. E., and A. J. Ukhorskiy (2001), Observations of electromagnetic ion cyclotron waves during geomagnetic storms: Wave occurrence and pitch angle scattering, *J. Geophys. Res.*, 106, 3883–3896, doi:10.1029/2000JA000083.
- Fraser, B. J., R. S. Grew, S. K. Morley, J. C. Green, H. J. Singer, T. M. Loto'aniu, and M. F. Thomsen (2010), Storm time observations of electromagnetic ion cyclotron waves at geosynchronous orbit: GOES results, *J. Geophys. Res.*, 115, A05208, doi:10.1029/2009JA014516.
- Friedel, R. H. W., G. D. Reeves, and T. Obara (2002), Relativistic electron dynamics in the inner magnetosphere—A review, *J. Atmos. Sol. Terr. Phys.*, 64, 265–282, doi:10.1016/S1364-6826(01)00088-8.
- Gao, Z., Z. Su, H. Zhu, F. Xiao, H. Zheng, Y. Wang, C. Shen, and S. Wang (2016), Intense low-frequency chorus waves observed by Van Allen probes: Fine structures and potential effect on radiation belt electrons, *Geophys. Res. Lett.*, 43, 967–977, doi:10.1002/2016GL067687.
- Green, J. C., T. G. Onsager, T. P. O'Brien, and D. N. Baker (2004), Testing loss mechanisms capable of rapidly depleting relativistic electron flux in the Earth's outer radiation belt, *J. Geophys. Res.*, 109, A12211, doi:10.1029/2004JA010579.
- He, F., X. Cao, B. Ni, Z. Xiang, C. Zhou, X. Gu, Z. Zhao, R. Shi, and Q. Wang (2016), Combined scattering loss of radiation belt relativistic electrons by simultaneous three-band EMIC waves: A case study, *J. Geophys. Res. Space Physics*, 121, 4446–4451, doi:10.1002/2016JA022483.
- Horne, R. B., and R. M. Thorne (1998), Potential waves for relativistic electron scattering and stochastic acceleration during magnetic storms, *Geophys. Res. Lett.*, 25, 3011–3014, doi:10.1029/98GL01002.
- Hudson, M. K., D. N. Baker, J. Goldstein, B. T. Kress, J. Paral, F. R. Toffoletto, and M. Wiltberger (2014), Simulated magnetopause losses and Van Allen probe flux dropouts, *Geophys. Res. Lett.*, 41, 1113–1118, doi:10.1002/2014GL059222.
- Inan, U. S., T. F. Bell, and R. A. Helliwell (1978), Nonlinear pitch angle scattering of energetic electrons by coherent VLF waves in the magnetosphere, *J. Geophys. Res.*, 83, 3235–3253, doi:10.1029/JA083iA07p03235.
- Jordanova, V. K., J. Albert, and Y. Miyoshi (2008), Relativistic electron precipitation by EMIC waves from self-consistent global simulations, *J. Geophys. Res.*, 113, A00A10, doi:10.1029/2008JA013239.
- Kennel, C. F., and F. Engelmann (1966), Velocity space diffusion from weak plasma turbulence in a magnetic field, *Phys. Fluids*, 9, 2377–2388, doi:10.1063/1.1761629.
- Kersten, T., R. B. Horne, S. A. Glauert, N. P. Meredith, B. J. Fraser, and R. S. Grew (2014), Electron losses from the radiation belts caused by EMIC waves, *J. Geophys. Res. Space Physics*, 119, 8820–8837, doi:10.1002/2014JA020366.
- Kim, H.-J., and A. A. Chan (1997), Fully adiabatic changes in storm time relativistic electron fluxes, *J. Geophys. Res.*, 102, 22,107–22,116, doi:10.1029/97JA01814.
- Lemons, D. S. (2012), Pitch angle scattering of relativistic electrons from stationary magnetic waves: Continuous Markov process and quasilinear theory, *Phys. Plasmas*, 19(1), 012306.
- Li, W., Y. Y. Shprits, and R. M. Thorne (2007), Dynamic evolution of energetic outer zone electrons due to wave-particle interactions during storms, *J. Geophys. Res.*, 112, A10220, doi:10.1029/2007JA012368.
- Li, X., D. N. Baker, M. Temerin, T. E. Cayton, E. G. D. Reeves, R. A. Christensen, J. B. Blake, M. D.Looper, R. Nakamura, and S. G. Kanekal (1997), Multisatellite observations of the outer zone electron variation during the November 3–4, 1993, magnetic storm, *J. Geophys. Res.*, 102, 14,123–14,140, doi:10.1029/97JA01101.
- Liu, K., D. S. Lemons, D. Winske, and S. P. Gary (2010), Relativistic electron scattering by electromagnetic ion cyclotron fluctuations: Test particle simulations, *J. Geophys. Res.*, 115, A04204, doi:10.1029/2009JA014807.
- Liu, K., D. Winske, S. P. Gary, and G. D. Reeves (2012), Relativistic electron scattering by large amplitude electromagnetic ion cyclotron waves: The role of phase bunching and trapping, *J. Geophys. Res.*, 117, A06218, doi:10.1029/2011JA017476.
- Loto'aniu, T. M., B. J. Fraser, and C. L. Waters (2005), Propagation of electromagnetic ion cyclotron wave energy in the magnetosphere, *J. Geophys. Res.*, 110, A07214, doi:10.1029/2004JA010816.
- Loto'aniu, T. M., H. J. Singer, C. L. Waters, V. Angelopoulos, I. R. Mann, S. R. Elkington, and J. W. Bonnell (2010), Relativistic electron loss due to ultralow frequency waves and enhanced outward radial diffusion, *J. Geophys. Res.*, 115, A12245, doi:10.1029/2010JA015755.
- Lyons, L. R. (1974), General relations for resonant particle diffusion in pitch angle and energy, *J. Plasma Phys.*, 12, 45–49, doi:10.1017/S0022377800024910.
- Lyons, L. R., and D. J. Williams (1984), *Quantitative Aspects of Magnetospheric Physics*, Springer, New York.
- Lyons, L. R., R. M. Thorne, and C. F. Kennel (1971), Electron pitch-angle diffusion driven by oblique whistler-mode turbulence, *J. Plasma Phys.*, 6, 589–606, doi:10.1017/S0022377800006310.
- Matsuomoto, H., and Y. Omura (1981), Cluster and channel effect phase bunchings by whistler waves in the nonuniform geomagnetic field, *J. Geophys. Res.*, 86, 779–791, doi:10.1029/JA086iA02p00779.
- McIlwain, C. E. (1966), Ring current effects on trapped particles, *J. Geophys. Res.*, 71, 3623–3628, doi:10.1029/JZ071i015p03623.
- Meredith, N. P., R. M. Thorne, R. B. Horne, D. Summers, B. J. Fraser, and R. R. Anderson (2003), Statistical analysis of relativistic electron energies for cyclotron resonance with EMIC waves observed on CRRES, *J. Geophys. Res.*, 108, 1250, doi:10.1029/2002JA009700.
- Millan, R. M., and R. M. Thorne (2007), Review of radiation belt relativistic electron losses, *J. Atmos. Sol. Terr. Phys.*, 69, 362–377, doi:10.1016/j.jastp.2006.06.019.
- Min, K., J. Lee, K. Keika, and W. Li (2012), Global distribution of EMIC waves derived from THEMIS observations, *J. Geophys. Res.*, 117, A05219, doi:10.1029/2012JA017515.
- Miyoshi, Y., K. Sakaguchi, K. Shiokawa, D. Evans, J. Albert, M. Connors, and V. Jordanova (2008), Precipitation of radiation belt electrons by EMIC waves, observed from ground and space, *Geophys. Res. Lett.*, 35, L23101, doi:10.1029/2008GL035727.
- Mourenas, D., A. V. Artemyev, Q. Ma, O. V. Agapitov, and W. Li (2016), Fast dropouts of multi-MeV electrons due to combined effects of EMIC and whistler-mode waves, *Geophys. Res. Lett.*, 43, 4155–4163, doi:10.1002/2016GL068921.
- Omura, Y., and Q. Zhao (2012), Nonlinear pitch-angle scattering of relativistic electrons by EMIC waves in the inner magnetosphere, *J. Geophys. Res.*, 117, A08227, doi:10.1029/2012JA017943.
- Omura, Y., Y. Katoh, and D. Summers (2008), Theory and simulation of the generation of whistler-mode chorus, *J. Geophys. Res.*, 113, A04223, doi:10.1029/2007JA012622.
- Omura, Y., J. Pickett, B. Grison, O. Santolik, I. Dandouras, M. Engebretson, P. M. E. Décréau, and A. Masson (2010), Theory and observation of electromagnetic ion cyclotron triggered emissions in the magnetosphere, *J. Geophys. Res.*, 115, A07234, doi:10.1029/2010JA015300.
- Omura, Y., Y. Miyashita, M. Yoshikawa, D. Summers, M. Hikishima, Y. Ebihara, and Y. Kubota (2015), Formation process of relativistic electron flux through interaction with chorus emissions in the Earth's inner magnetosphere, *J. Geophys. Res. Space Physics*, 120, 9545–9562, doi:10.1002/2015JA021563.

- Pickett, J. S., et al. (2010), Cluster observations of EMIC triggered emissions in association with Pc1 waves near Earth's plasmapause, *Geophys. Res. Lett.*, 37, L09104, doi:10.1029/2010GL042648.
- Qin, G., and A. Shalchi (2009), Pitch-angle diffusion coefficients of charged particles from computer simulations, *Astrophys. J.*, 707(1), 61–66.
- Ragot, B. (2012), Nonresonant interaction of charged energetic particles with low-frequency noncompressive turbulence: Numerical simulation, *Astrophys. J.*, 758(2), 89.
- Reeves, G. D., R. H. W. Friedel, R. D. Belian, M. M. Meier, M. G. Henderson, T. Onsager, H. J. Singer, D. N. Baker, X. Li, and J. B. Blake (1998), The relativistic electron response at geosynchronous orbit during the January 1997 magnetic storm, *J. Geophys. Res.*, 103, 17,559–17,570, doi:10.1029/97JA03236.
- Rodger, C. J., A. T. Hendry, M. A. Clilverd, C. A. Kletzing, J. B. Brundell, and G. D. Reeves (2015), High-resolution in situ observations of electron precipitation-causing EMIC waves, *Geophys. Res. Lett.*, 42, 9633–9641, doi:10.1002/2015GL066581.
- Saikin, A. A., J.-C. Zhang, R. C. Allen, C. W. Smith, L. M. Kistler, H. E. Spence, R. B. Torbert, C. A. Kletzing, and V. K. Jordanova (2015), The occurrence and wave properties of H<sup>+</sup>-, He<sup>+</sup>-, and O<sup>+</sup>-band EMIC waves observed by the Van Allen Probes, *J. Geophys. Res.*, 120, 7477–7492, doi:10.1002/2015JA021358.
- Schulz, M., and L. J. Lanzerotti (1974), Particle diffusion in the radiation belts, in *Physics and Chemistry in Space*, vol. 7, 215 pp., Springer, New York.
- Shprits, Y. Y., R. M. Thorne, R. Friedel, G. D. Reeves, J. Fennell, D. N. Baker, and S. G. Kanekal (2006), Outward radial diffusion driven by losses at magnetopause, *J. Geophys. Res.*, 111, A11214, doi:10.1029/2006JA011657.
- Shprits, Y. Y., D. Subbotin, and B. Ni (2009a), Evolution of electron fluxes in the outer radiation belt computed with the VERB code, *J. Geophys. Res.*, 114, A11209, doi:10.1029/2008JA013784.
- Shprits, Y. Y., L. Chen, and R. M. Thorne (2009b), Simulations of pitch angle scattering of relativistic electrons with MLT-dependent diffusion coefficients, *J. Geophys. Res.*, 114, A03219, doi:10.1029/2008JA013695.
- Su, Z., H. Zheng, and S. Wang (2009), Evolution of electron pitch angle distribution due to interactions with whistler-mode chorus following substorm injections, *J. Geophys. Res.*, 114, A08202, doi:10.1029/2009JA014269.
- Su, Z., F. Xiao, H. Zheng, and S. Wang (2010a), Combined radial diffusion and adiabatic transport of radiation belt electrons with arbitrary pitch-angles, *J. Geophys. Res.*, 115, A10249, doi:10.1029/2010JA015903.
- Su, Z., H. Zheng, and S. Wang (2010b), Three dimensional simulations of energetic outer zone electron dynamics due to wave-particle interaction and azimuthal advection, *J. Geophys. Res.*, 115, A06203, doi:10.1029/2009JA014980.
- Su, Z., F. Xiao, H. Zheng, and S. Wang (2010c), STEERB: A three-dimensional code for storm-time evolution of electron radiation belt, *J. Geophys. Res.*, 115, A09208, doi:10.1029/2009JA015210.
- Su, Z., F. Xiao, H. Zheng, and S. Wang (2011a), CRRES observation and STEERB simulation of the 9 October 1990 electron radiation belt dropout event, *Geophys. Res. Lett.*, 38, L06106, doi:10.1029/2011GL046873.
- Su, Z., H. Zheng, L. Chen, and S. Wang (2011b), Numerical simulations of storm-time outer radiation belt dynamics by wave-particle interactions including cross diffusion, *J. Atmos. Sol. Terr. Phys.*, 73, 95–105, doi:10.1016/j.jastp.2009.08.002.
- Su, Z., H. Zhu, F. Xiao, H. Zheng, C. Shen, Y. Wang, and S. Wang (2012), Bounce-averaged advection and diffusion coefficients for monochromatic electromagnetic ion cyclotron wave: Comparison between test-particle and quasi-linear models, *J. Geophys. Res.*, 117, A09222, doi:10.1029/2012JA017917.
- Su, Z., H. Zhu, F. Xiao, H. Zheng, C. Shen, Y. Wang, and S. Wang (2013a), Latitudinal dependence of nonlinear interaction between electromagnetic ion cyclotron wave and radiation belt relativistic electrons, *J. Geophys. Res. Space Physics*, 118, 3188–3202, doi:10.1002/jgra.50289.
- Su, Z., H. Zhu, F. Xiao, H. Zheng, C. Shen, Y. Wang, and S. Wang (2013b), Latitudinal dependence of nonlinear interaction between electromagnetic ion cyclotron wave and radiation belt relativistic electrons, *J. Geophys. Res. Space Physics*, 118, 3188–3202, doi:10.1002/jgra.50289.
- Su, Z., et al. (2014a), Nonstorm time dynamics of electron radiation belts observed by the Van Allen Probes, *Geophys. Res. Lett.*, 41, 229–235, doi:10.1002/2013GL058912.
- Su, Z., H. Zhu, F. Xiao, H. Zheng, M. Zhang, Y. C.-M. Liu, C. Shen, Y. Wang, and S. Wang (2014b), Latitudinal dependence of nonlinear interaction between electromagnetic ion cyclotron wave and terrestrial ring current ions, *Phys. Plasmas*, 21(5), 052310, doi:10.1063/1.4880036.
- Su, Z., et al. (2015), Ultra-low-frequency wave-driven diffusion of radiation belt relativistic electrons, *Nat. Commun.*, 6, 10096, doi:10.1038/ncomms10096.
- Su, Z., et al. (2016), Nonstorm time dropout of radiation belt electron fluxes on 24 September 2013, *J. Geophys. Res. Space Physics*, 121, 6400–6416, doi:10.1002/2016JA022546.
- Summers, D. (2005), Quasi-linear diffusion coefficients for field-aligned electromagnetic waves with applications to the magnetosphere, *J. Geophys. Res.*, 110, A08213, doi:10.1029/2005JA011159.
- Summers, D., and Y. Omura (2007), Ultra-relativistic acceleration of electrons in planetary magnetospheres, *Geophys. Res. Lett.*, 34, L24205, doi:10.1029/2007GL032226.
- Summers, D., and R. M. Thorne (2003), Relativistic electron pitch-angle scattering by electromagnetic ion cyclotron waves during geomagnetic storms, *J. Geophys. Res.*, 108, 1143, doi:10.1029/2002JA009489.
- Summers, D., R. M. Thorne, and F. Xiao (1998), Relativistic theory of wave-particle resonant diffusion with application to electron acceleration in the magnetosphere, *J. Geophys. Res.*, 103, 20,487–20,500, doi:10.1029/98JA01740.
- Summers, D., B. Ni, and N. P. Meredith (2007), Timescales for radiation belt electron acceleration and loss due to resonant wave-particle interactions: 2. Evaluation for VLF chorus, ELF hiss, and electromagnetic ion cyclotron waves, *J. Geophys. Res.*, 112, A04207, doi:10.1029/2006JA011993.
- Tao, X., and J. Bortnik (2010), Nonlinear interactions between relativistic radiation belt electrons and oblique whistler mode waves, *Nonlinear Processes Geophys.*, 17, 599–604, doi:10.5194/npg-17-599-2010.
- Thorne, R. M. (2010), Radiation belt dynamics: The importance of wave-particle interactions, *Geophys. Res. Lett.*, 37, L22107, doi:10.1029/2010GL044990.
- Thorne, R. M., and C. F. Kennel (1971), Relativistic electron precipitation during magnetic storm main phase, *J. Geophys. Res.*, 76, 4446–4453, doi:10.1029/JA076i019p04446.
- Turner, D. L., Y. Shprits, M. Hartinger, and V. Angelopoulos (2012), Explaining sudden losses of outer radiation belt electrons during geomagnetic storms, *Nat. Phys.*, 8, 208–212, doi:10.1038/nphys2185.
- Turner, D. L., et al. (2014), On the cause and extent of outer radiation belt losses during the 30 September 2012 dropout event, *J. Geophys. Res. Space Physics*, 119, 1530–1540, doi:10.1002/2013JA019446.

- Ukhorskiy, A. Y., Y. Y. Shprits, B. J. Anderson, K. Takahashi, and R. M. Thorne (2010), Rapid scattering of radiation belt electrons by storm-time EMIC waves, *Geophys. Res. Lett.*, 37, L09101, doi:10.1029/2010GL042906.
- Usanova, M. E., et al. (2014), Effect of EMIC waves on relativistic and ultrarelativistic electron populations: Ground-based and Van Allen Probes observations, *Geophys. Res. Lett.*, 41, 1375–1381, doi:10.1002/2013GL059024.
- Wang, B., Z. Su, Y. Zhang, S. Shi, and G. Wang (2016), Nonlinear Landau resonant scattering of near-equatorially mirroring radiation belt electrons by oblique EMIC waves, *Geophys. Res. Lett.*, 43, 3628–3636, doi:10.1002/2016GL068467.
- Zhang, X.-J., et al. (2016), Direct evidence for EMIC wave scattering of relativistic electrons in space, *J. Geophys. Res. Space Physics*, 121, 6620–6631, doi:10.1002/2016JA022521.
- Zhu, H., Z. Su, F. Xiao, H. Zheng, C. Shen, Y. Wang, and S. Wang (2012), Nonlinear interaction between ring current protons and electromagnetic ion cyclotron waves, *J. Geophys. Res.*, 117, A12217, doi:10.1029/2012JA018088.
- Zhu, H., et al. (2015), Plasmatrough exohiss waves observed by Van Allen Probes: Evidence for leakage from plasmasphere and resonant scattering of radiation belt electrons, *Geophys. Res. Lett.*, 42, 1012–1019, doi:10.1002/2014GL062964.